Available online at www.sciencedirect.com
SCIENCE DIRECT®
Acta Materialia 52 (2004) 4659–4668
Acta MATERIALIA
www.actamat-journals.com

Modeling the dynamic recrystallization under multi-stage hot deformation

G. Kugler *, R. Turk

Faculty of Natural Sciences and Engineering, University of Ljubljana, Aškerčeva cesta 012, 1000 Ljubljana, Slovenia

Received 3 November 2003; received in revised form 8 June 2004; accepted 11 June 2004
Available online 15 July 2004

Abstract

The kinetics of the restoration processes that take place during the isothermal annealing of metals for the case when the critical strain for the onset of dynamic recrystallization is reached and exceeded were modeled using the Cellular Automata approach. The model enables both quantitative and topographic simulations of microstructural evolution before and during metadynamic recrystallization. It allows the simulation of multi-stage deformation. It was observed that two kinds of transition between the strain-dependent and strain-independent range are possible: the first is smooth, whereas the second is oscillatory. The post-dynamic softening is shown to be weakly dependent on strain and temperature, but strongly dependent on strain rate, as has been observed in published experimental work.

Keywords: Dynamic recrystallization; Metadynamic recrystallization; Modeling; Cellular automaton; Hot working

1. Introduction

Multi-pass processing is very common in the hot deformation of metals. The control of such operations is only possible when a knowledge of the microstructural changes and the softening mechanisms taking place during the passes is available. Only in this way can we successfully predict and achieve the desirable mechanical properties of the final product. For the plastic deformation of metals and alloys at high temperature, two types of behavior are possible. For high-stacking-fault-energy materials, such as α-iron, Al, etc., a dynamic equilibrium between the generation and accumulation of dislocations, on the one hand, and annihilation by rearrangement, on the other, is maintained. Therefore, a constant flow stress is reached after a certain amount of deformation. For the low- and medium-stacking-fault-energy materials, such as copper, nickel, γ-iron, austenitic steel, etc., a much higher storage rate is reached due to their lower rate of dynamic recovery (DRV). At the same time, small dislocation-free regions are produced, which can grow into surrounding material that contain dislocations. Such recrystallized regions are separated from the surrounding material by high-angle boundaries. This generation of nuclei and growth is called dynamic recrystallization (DRX).

If deformation is interrupted before the strain, ε_c, for the onset of DRX is reached, then static recrystallization (SRX) takes place. SRX is nucleated preferentially at the original grain boundaries, and these dislocation-free regions grow until impingement [1]. The kinetics of SRX is strongly dependent on strain and temperature, but less on the strain rate. Whenever ε_c is reached and exceeded during hot deformation, a different type of recrystallization, referred to as metadynamic recrystallization (MDRX), takes place, which is a strong function of the strain rate and a weak function of the strain and temperature [2]. MDRX can start immediately after deformation without any incubation period, because once DRX occurs there are always nuclei present in the material. Since the 1960s a great deal of effort has focused on trying to explain and describe the dynamic and

* Corresponding author. Tel.: +386-142-503-16; fax: +386-147-045-60.
E-mail address: goran.kugler@uni-lj.si (G. Kugler).

1359-6454/$30.00 © 2004 Acta Materialia Inc. Published by Elsevier Ltd. All rights reserved.
doi:10.1016/j.actamat.2004.06.022

post-dynamic behavior of metallic materials during hot working [2–14]. Many research studies attempted to develop models, based mainly on the JMAK equation approach, to describe the phenomena [3–8]. The importance of the subject is also reflected in the large body of reported experimental studies [6–14].

Recently, Roucoules et al. [15] performed simulations of DRX and post-dynamic behavior based on the Sandström and Lagneborg approach [16,17]. Uranga et al. [18] experimentally researched the dependence of softening on prior strain. All these results and the importance of the topic were the motivation for the present work. The aim of this paper is to analyze post-dynamic softening behavior under various deformation conditions for the case when the critical strain, ε_c, for the onset of DRX is reached and exceeded. Special attention is given to a detailed consideration of the dependence of the time for 50% recrystallization on previous deformation, as well as the influence of recovery on the post-dynamic kinetics.

2. Modeling

In order to simulate recrystallization the Cellular Automata (CA) method was selected. The CA method was first proposed by von Neumann for a complex systems, and it has since been applied to a wide range of phenomena. The CA method for simulating primary recrystallization was first introduced by Hesselbarth and Göbel [19], while Goetz and Seetharaman [20] were the first to use it to simulate DRX. This study involves a generalization of previous CA models [20,24,25] for hot working occurring by DRX to recrystallization after hot working. Here the use of the CA method to model the post-dynamic recrystallization, when DRX is initiated during deformation, is now introduced and presented for the first time to the best of the author's knowledge.

The CA method discretizes the space of interest into lattice elements called cells. The state of every cell is determined by the states of neighboring cells, $N(C)$, and the cell C itself. The evolution of the system is determined according to the transformation rule F, which computes the new states of all the cells and could be either deterministic or probabilistic. The value of the state vector, Ψ, of an arbitrary cell at time t can be expressed as

$$\Psi^t(C) = F(\Psi^{t-\Delta t}(N(C)), \Psi^{t-\Delta t}(C)). \tag{1}$$

For a detailed explanation and general information about CA theory, as well as for the CA simulation technique, the reader is referred to [21–23].

In this paper, a 2-D square lattice was employed. Every cell has four state variables: one grain number variable that represents different grains, one orientation variable that represents the grain boundary-energy, one dislocation-density variable and one distance variable that controls grain-boundary movement. In order to simulate equiaxial grain growth, a probabilistic transformation rule [23–25] and the von Neumann neighboring rule were used. The dependence of the dislocation density, ρ, of a particular cell on the shear strain, γ, is given by

$$\frac{\mathrm{d}\rho}{\mathrm{d}\gamma} = k_1\sqrt{\rho} - k_2\rho, \tag{2}$$

which is the Kocks and Mecking law [1,26] at the macroscopic level, where k_1 is a constant that represents hardening, and k_2 is the softening parameter that represents recovery of dislocations and is temperature and strain-rate dependent. The high-temperature flow stress is related to the density of dislocations within the grain by [1,26]

$$\sigma = \alpha G b\sqrt{\bar{\rho}}, \tag{3}$$

where α is a dislocation-interaction term, which is 0.5–1.0 for most metals, G is the shear modulus and b is Burger's vector. The average dislocation density, $\bar{\rho}$, is associated with the dislocation densities, ρ_i, of all the cells by the following equation:

$$\bar{\rho} = \frac{1}{n}\sum_{i=1}^{n}\rho_i, \tag{4}$$

where n is the total number of cells. It is generally assumed for the pure metals [1] that the velocity of grain-boundary movement fulfills the following relation:

$$v = M\Delta f, \tag{5}$$

where Δf is the driving force per unit area and M is the grain-boundary mobility, which can be calculated with [24,27]

$$M = \frac{b\delta D}{kT}\exp\left(\frac{Q_b}{RT}\right), \tag{6}$$

where δ is the characteristic grain-boundary thickness, D_b is the boundary self-diffusion coefficient, Q_b is the boundary-diffusion activation energy and k is Boltzmann's constant. The driving force depends on the dislocation-density difference, $\Delta\rho$, between a growing grain and the grain into which the grain grows, and on the grain-boundary energy, γ [1,24], thus

$$\Delta f = \tau\Delta\rho - 2\gamma/r, \tag{7}$$

where $\tau = \mu b^2/2$ is the dislocation line energy. If we make the simplifying assumption that the boundary energy is primarily a function of the boundary misorientation, the grain-boundary energy, γ, can be calculated from the well-known Read–Shockley equation [1,28]

$$\gamma = \gamma_m\frac{\theta}{\theta_m}\left(1 - \ln\left(\frac{\theta}{\theta_m}\right)\right), \tag{8}$$

where θ is the grain-boundary misorientation, γ_m and θ_m are the boundary energy and misorientation when the

Table 1
Values of parameters used in simulations

Q_b (kJ/mol)	δD_b ($m^3\ s^{-1}$)	α	G (Pa)	b (m)	γ_m (J m^2)
110	7.5×10^{-15}	0.5	4.21×10^{-10}	2.56×10^{-10}	0.625
Q_a (kJ/mol)	n	A (Pa^n)	ω (K)	k	zk_1 (m^{-1})
275	7.6	2.0×10^{44}	2100	8.0	2.97×10^8

grain boundary becomes a high-angle boundary and the boundary properties remain virtually independent of misorientation. The initial microstructure was created with a randomly generated predefined number of nuclei across the matrix and by allowing growth until impingement with other growing grains (site-saturated nucleation), which yields an approximately normal distribution of grain sizes. The mean grain diameter was defined by ASTM convention. Every primary and newly formed grain has an orientation in the range 0–π, which was set randomly. The dislocation density is identical for all primary grains and follows the evolution Eq. (2). For DRX grains the dislocation density also follows Eq. (2) with continued deformation. The time step, Δt, is defined as the ratio between the cell diameter, d, and maximum grain-boundary velocity, v_{max}. The maximum velocity is achieved by a grain that grows into a fully hardened grain at an early stage of its growth. Thus taking into account Eqs. (2), (5) and (7)

$$\Delta t = \frac{d}{v_{max}} = \frac{k_2^2 d}{M\tau k_1^2}. \tag{9}$$

At this point an additional factor, k_{GB}, is introduced, which enables a correction of the time evolution of grain-boundary velocity due to the probabilistic grain-boundary movement. This factor was determined for each simulation separately by comparing the time evolutions of growth velocities for the theoretical (Eq. (5)) and the simulated values associated with a single grain that grows into the fully hardened material ($k_{GB} \in [1.8, 2.4]$). The recovery parameter, k_2, can be calculated from an empirical expression that describes the dependence of peak stress on the temperature and strain rate $\sigma_p^n = A\dot{\varepsilon}\exp(Q_a/RT)$ as $k_2 = \alpha G b k_1/\sigma_p$, where n and A are constants, and Q_a activation energy [1,24]. The strain step, $\Delta\varepsilon$, is strain-rate dependent as $\Delta\varepsilon = \dot{\varepsilon}\Delta t$. A recrystallization event will occur at a cell when the following conditions are fulfilled simultaneously: (a) the cell is at a grain boundary; (b) the driving force is positive; (c) the computer-generated random number is less than the transformation probability p which is defined as $p = i/4$, where i is the number of neighboring cells transformed in the previous step [24]; (d) the distance variable is greater than the diameter of a cell. The distance variable is calculated as $r^t = r^{t-\Delta t} + v\Delta t$ when the cell is at a grain boundary. When recrystallization occurs the recrystallized cell obtains its orientation, grain number and dislocation density from the growing grain and the distance variable is set to zero. If the dislocation density at the grain boundary exceeds the critical value for dynamic recrystallization ρ_{cr}, a new nucleus is produced with probability $P(P = k\dot{\varepsilon}\exp(-\omega/T)\Delta t)$. For the new nucleus the dislocation density and the distance variable are set to zero. The nucleus also obtains a new grain number and a new random orientation. It is assumed that nucleation takes place on grain boundaries only. Other high-energy defects inside grains (e.g., deformation bands, dislocation tangles, subgrain walls, etc.), which could also act as nucleation sites, are neglected.

When deformation is interrupted, during each time step the new dislocation density inside each cell is calculated from its current dislocation density, ρ_c, from Eq. (2), where the hardening coefficient k_1 is set to zero. This yields an exponential decrease in dislocation density with time

$$\rho(\Delta t) = \rho_c \exp(-k_2\dot{\varepsilon}\Delta t). \tag{10}$$

Thus, static recovery in this model is assumed to only decrease the dislocation density inside each cell [29]. This will be further discussed in a later section. Otherwise, no other distinction is made between the dynamic and static processes. Thus the same governing Eqs. (3)–(8) are used for both simulations before and after interruption. However, instead of Eq. (2), Eq. (10) is used. The simulation grid consists of 700×700 cells with periodic boundary conditions. The size of a cell is 2 μm. The constants used in the simulations are collected in Table 1.

3. Results and discussion

Simulated, continuous stress–strain curves at a constant temperature and at various strain rates are presented in Fig. 1(a), and for constant strain rate and various temperatures in Fig. 1(b). The initial mean size of the primary grains, D_0, was 80 μm. A single-peak flow curve is produced at high strain rates and/or low temperatures (high values of the Zener–Hollomon parameter Z) and multiple peaks at low strain rates and/or high temperatures (low values of Z), which is consistent with experimental observations of DRX under hot-working conditions for metals [1,4,7–9].

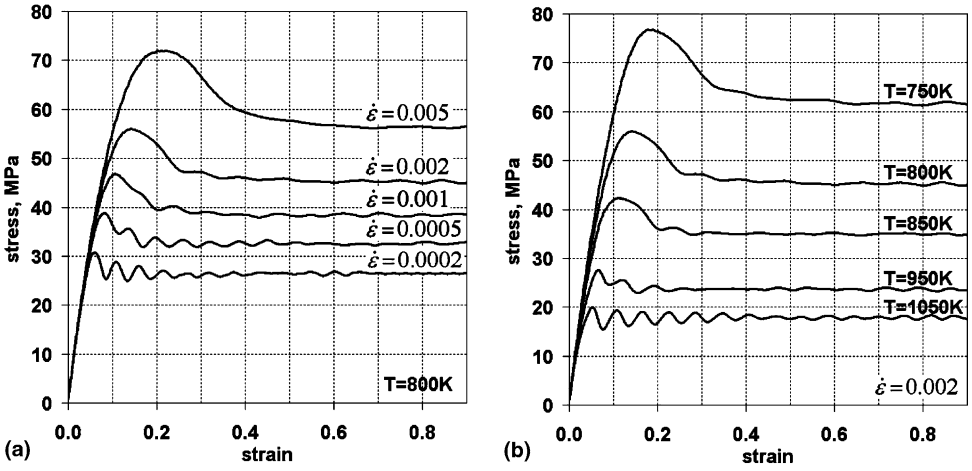

Fig. 1. Simulated continuous stress–strain curves for a temperature of 800 K and for different strain rates (a) and for a strain rate of 0.002 s^{-1} and different temperatures (b). The initial mean grain size was 80 μm.

An example of a simulated flow-stress curve (curve C1) for a two-stage experiment is shown in Fig. 2(a). The initial mean grain size was 80 μm, the temperature 750 K and the strain rate 0.002 s^{-1}. As the deformation proceeds, the dislocation density (or stress) increases until the critical density, ρ_{cr}, for the onset of DRX is reached, when nuclei appear on the original grain boundaries. New grains start to grow, but the concurrent work-hardening builds up the dislocation density inside them and reduces the driving force for boundary migration until the growth stops. At the same time, when the dislocation density in the new grains reaches ρ_{cr}, the next round of DRX can occur. This leads to necklace formation around pre-existing grain boundaries, as shown in the simulated microstructure at a strain of 0.17 in Fig. 3(a). With a further increase in strain the curve reaches its maximum and then starts to decrease toward the steady-state stress, which, for a given material, is uniquely determined by the temperature compensated strain rate Z. As complementary information, the mean-grain-size evolution for the same simulation is displayed in Fig. 2(b). The abscissa on this graph represents time, t. The mean grain size, D, quickly drops from an initial size D_0 toward the steady-state size, D_{ss}, which is 15.4 μm for the current thermo-mechanical conditions, and is also uniquely determined by the temperature compensated strain rate.

The deformation was interrupted at $\varepsilon = 0.4$ (point A on both figures) and post-dynamic softening began to operate. The mean grain size at that moment was 16.5 μm and old grains were completely consumed by new DRX grains (see the microstructure in Fig. 3(b)). Nuclei that are created during deformation rapidly grow since there is no concurrent hardening. Partially hardened grains also continue to grow. Nucleation takes place at the grain boundaries of fully hardened grains until all the nucleation sites are exhausted. At the same time, fully and partially hardened grains are softened by static

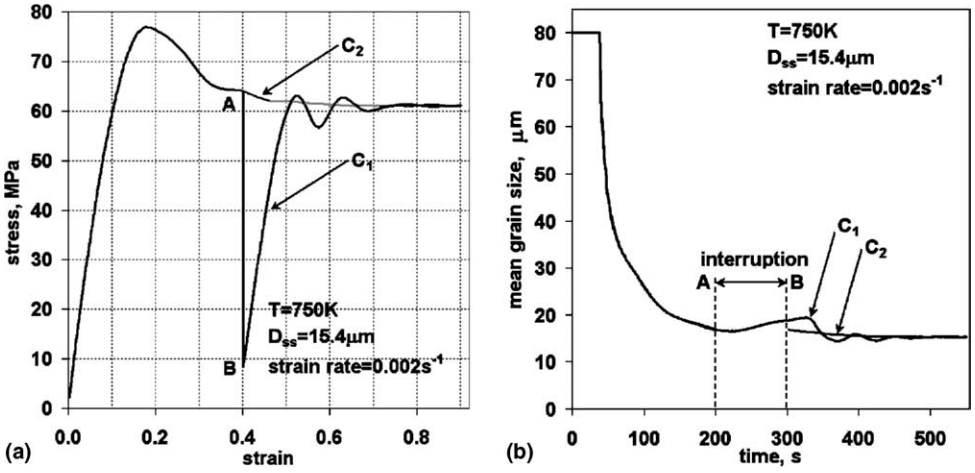

Fig. 2. Simulated flow curve for two-stage experiment (a) and the evolution of mean grain size with time (b) for an initial mean grain size of 80 μm at a strain rate of 0.002 s^{-1} and temperature of 750 K.

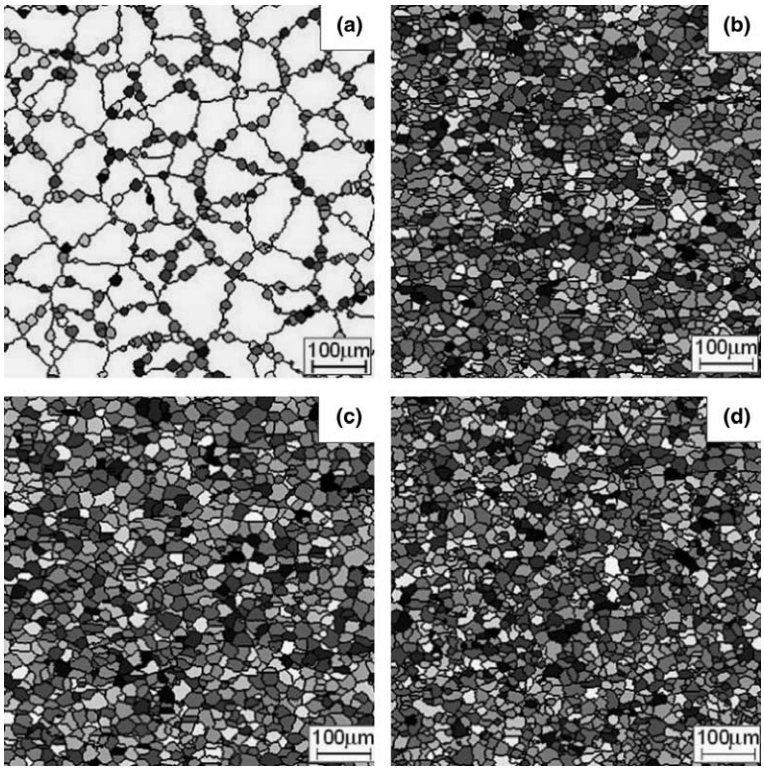

Fig. 3. Simulated microstructure at strains of 0.17 (a) and of 0.4 (b), just before interruption (point A in Fig. 2), of 0.4 (c), after holding for 100 s at a temperature of 750 K (point B in Fig. 2) and at a strain of 0.9 (d) in the steady-state area, which is the same as obtained for the simulation without interruption.

recovery. All those growing grains grow until impingement or until the driving force for grain-boundary migration is positive. The mean grain size increases and after 100 s (point B) it reaches the value of 19 μm, when deformation starts to operate again. The microstructure at this time is displayed in Fig. 3(c), where enlargement of the mean grain size is clearly seen. The dislocation density increases with increasing strain until ρ_{cr} is reached again and DRX starts. The strain rate and temperature were the same as in the first stage, but here the flow curve displays multiple-peak behavior. At the end, the flow-stress curve reaches the same steady-state value as it would have reached without interruption. The microstructure at the end of the simulated deformation is shown in Fig. 3(d). Note that in both Figs. 2(a) and (b), the curves for continuous deformation are added and labeled as C2 (gray lines). The reason for the above-mentioned transition from a single peak to multiple peaks after the interruption is grain refinement, and is in agreement with Sakai et al. [4,9], who found experimentally that single-peak behavior is associated with grain refinement and multiple peaks with grain coursing. If $D_0/D_{ss} > 2$ then single-peak flow stress is observed. In contrast, when $D_0/D_{ss} < 2$ there are a sufficient number of grain boundaries suitable for nucleation and new grains can develop at about the same rate, which leads to oscillations of the stress–strain curve. This effect of initial grain size on the shape of the flow-stress curves is presented in Fig. 4(a), where simulations were run for four different initial grain sizes at a temperature of 800 K and a strain rate of 0.002 s^{-1}. It can also be seen that the peak flow stress is higher for larger D_0, and that the steady-state stress is insensitive to D_0, which is in agreement with experimental observations [4] and with previously published results of CA simulations [20,24,25]. Fig. 4(b) shows all the corresponding mean-grain-size evolutions with strain, which all reach the same steady-state value of 18 μm, irrespective of D_0.

Two of the most important quantities, which for given TM conditions are mainly responsible for determining the kinetics of the post-dynamic softening, are the topology of the underlying microstructure and the spatial distribution of the dislocation density $g(\rho, t)$ across the sample at the time of interruption. The number of nucleation sites is dependent on the topology, and the velocity of the growing grains depends on the dislocation density, which provides the driving force for grain growth. Both quantities can be followed using the model, both during and after deformation. An example of how $g(\rho, \varepsilon)$ changes with strain for single-peak behavior is presented in Fig. 5(a). The corresponding flow-stress curve is given in Fig. 1. At $\varepsilon = 0$, the dislocation density is constant and equal for all the primary grains,

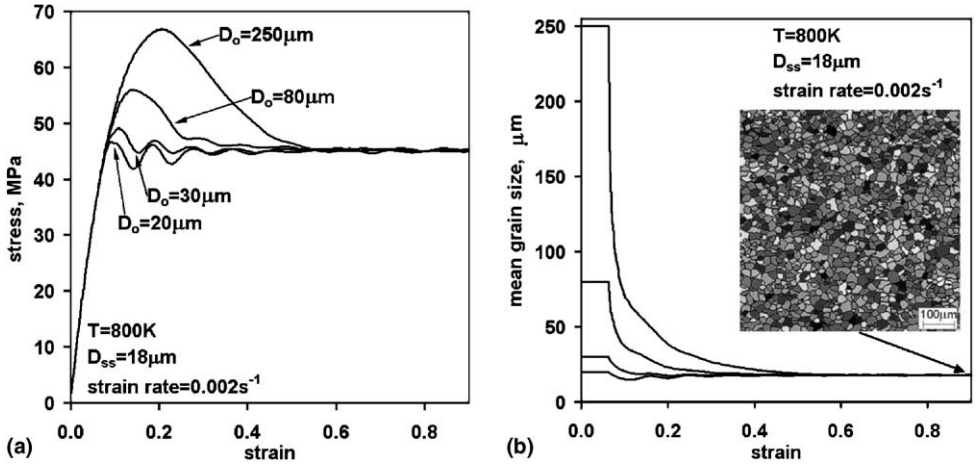

Fig. 4. Simulated stress–strain curves (a) and dependence of mean grain size on applied strain (b) for different initial mean grain sizes at strain rate of 0.002 s^{-1} and temperature of 800 K. The inset (b) shows the steady-state microstructure.

and the distribution function is given by $g(\rho,0) = \delta(\rho-\rho_{02})$, where δ is the Dirac delta function and ρ_{02} is a constant. Before the critical dislocation density is reached, the material deforms homogeneously and the delta function moves toward higher values of ρ ($g(\rho,\varepsilon) = \delta(\rho-\rho(\varepsilon))$). After DRX has started, the delta function starts to diminish and the distribution of ρ throughout the material becomes more and more heterogeneous (histogram 1) but with a very sharp boundary of $g(\rho,\varepsilon)$, which indicates to what degree the DRX grains that initially nucleated are hardened during the current deformation. Histogram 1 represents the distribution $g(\rho,\varepsilon=0.2)$, which consists of the two parts shown by the two arrows. The left part represents the recrystallized material and the right is the δ function, which represents unrecrystallized material. Its position indicates to what degree unrecrystallized material is hardened. The fraction of unrecrystallized material at this stage is $\int g(\rho')\delta(\rho'-\rho(\varepsilon))\,\mathrm{d}\rho'$. With progressing deformation the front edge of $g(\rho,\varepsilon)$ for DRX grains becomes smaller (histogram 2 $g(\rho,\varepsilon=0.3)$), but the distribution still consists of two parts. The position of the δ function is at the maximum ρ for current TM conditions. With progressing deformation the δ function does not move any more, but gets smaller until it disappears when all the material is recrystallized (histogram 3). When the steady-state strain, ε_{ss}, is reached, $g(\rho,\varepsilon)$ becomes practically insensitive to any further increase in strain. For multiple-peak behavior the time evolution of the dislocation-density distribution function consists of traveling dislocation-density waves before a steady state is reached.

When deformation is interrupted, the share of the cells with low ρ begins to grow at the expense of the cells with high ρ (see Fig. 5(b)). Histogram 1 shows $g(\rho,t=1s)$, which with time becomes more and more concentrated around smaller values of ρ (histogram 2 and 3). The distribution function contracts with time

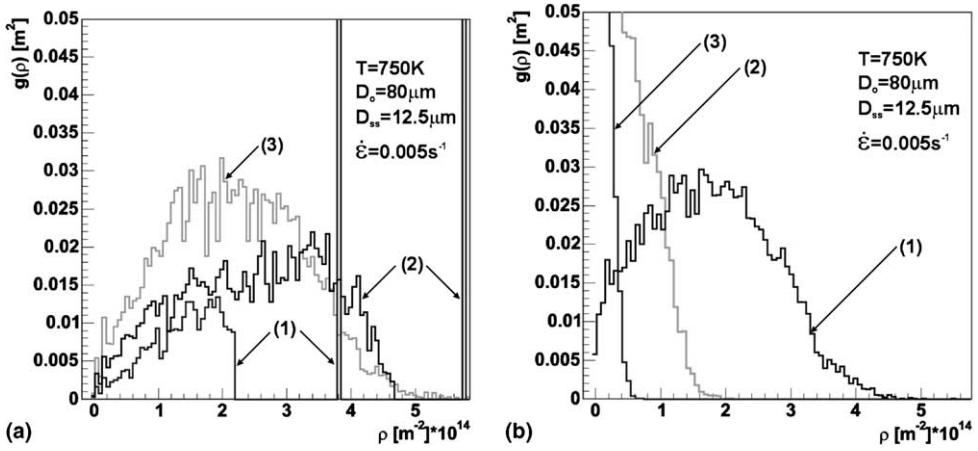

Fig. 5. Simulated evolution of the dislocation-density distribution function $g(\rho,t)$ during deformation (a) and between interruption (b). Numbers mark different stages of deformation (a) and different times after interruption (b). All distributions are normalized with condition $\int_0^\infty g(\rho,t)\,\mathrm{d}\rho = 1$.

toward the delta function that represents a completely annealed material ($g(\rho,\infty)=\delta(\rho-\rho_{02})$). The shape of the $g(\rho,\varepsilon)$ at the time of interruption will have a major influence on the kinetics of the post-dynamic softening.

Taking into account Eq. (3) the post-dynamic kinetics were followed by calculating the softening fraction as a function of time in the following way [30]:

$$X(t)=\frac{\sqrt{\rho_{\mathrm{m}}}-\sqrt{\rho(t)}}{\sqrt{\rho_{\mathrm{m}}}-\sqrt{\rho_{02}}}, \tag{11}$$

where ρ_{m} is the dislocation density at the moment of interruption, $\rho(t)$ is the dislocation density at the time t and ρ_{02} is a constant that is independent of strain rate or temperature and represents the point σ_{02}. Note that this is the value that was set for all the cells before the deformation began ($\rho_{02}=10^{10}$ m^{-2}). In reality this is not the case, as point σ_{02} is both strain-rate and temperature dependent.

The curves for the softening fraction obtained in this way for different temperatures and constant strain rate, and for different strain rates and constant temperature as a function of interrupted time, are presented in Figs. 6(a) and (b), respectively. They have typical sigmoidal shapes. It can be seen that an increase in strain rate by an order of magnitude is accompanied by an increase in the rate of softening by almost an order in magnitude (Fig. 6(b)). Increasing the temperature from 750 to 950 K does not affect the kinetics as much (Fig. 6(a)). Here we must also consider the simplification in Eq. (10), where ρ_{02} was taken as a constant. If strain-rate and temperature dependence are taken into account then the softening curves in Fig. 6(a) should be closer together, and they should be further apart in Fig. 6(b). This means an even stronger dependence on strain rate and a much weaker dependence on temperature than are shown. The Avrami plots for these curves are presented in Fig. 6(c). The straight lines indicate that the JMAK equation is followed. The line slopes corresponding to the time exponent are $\approx$1.0, and are virtually independent of the deformation parameters. However, there is a deviation from linearity for longer times. Again, these results are supported by published experimental work [3,5,10,18]. All the softening curves in Fig. 6(a)–(c) are taken at $\varepsilon=0.8$, where for all T and $\dot{\varepsilon}$ considered here the steady state is reached, so a comparison is possible.

The influence of static recovery on the recrystallization kinetics was also studied. Simulations were run with the coefficient k_2 in Eq. (10) set to zero. It was observed that recovery shifts the softening curves toward shorter times, on the one hand, and retards the growth of grains, on the other. As a consequence, the mean size of the MDRX grains was larger when the simulations where run without static recovery. This can be seen in Fig. 6(d), where the time evolution of the mean grain size for a constant strain rate of 0.002 s^{-1}, a temperature of 750 K and an initial grain size $D_0=80$ μm, is compared for simulations with and without recovery. The difference of 19.2 μm with recovery and of 25.4 μm without recovery, 500 s after interruption, is evident. The mean grain size at the time of interruption was 16.5 μm. The softening curves' shift toward shorter times for the simulation without static recovery (curve 1) compared to the simulation with recovery (curve 2), is presented in Fig. 7(d). Note that curve 1 does not achieve complete softening.

Rocoules et al. [10] in their simulations used the same equation for recovery during and after deformation. In contrast, Sandström and Lagneborg [17] neglected static recovery in their analysis. Both approaches were tested here (e.g., Figs. 6(d) and 7). Luton et al. [3] stated in their approach that the recovery process is comprised of two sequential mechanisms. The second, which cannot start before the first is completed, involves thermally activated unpinning or some diffusion-related processes in the neighborhood of the sub-boundaries, and leads to significant recovery. The first leads to a smaller degree of dislocation annihilation and involves the travelling of dislocations from dynamic to static obstacles. In their model the incubation time is introduced. Furthermore, Sakai et al. [4,9] introduced two types of recovery operating after interruption. The recovery in growing DRX grains is referred as metadynamic recovery (MDRV) and the recovery in fully hardened grains is referred to as static recovery (SRV). Clearly, these aspects require further investigation in order to incorporate an appropriate model of static recovery into our model.

The influence of deformation on the recrystallization kinetics is shown in Fig. 7, where the time for 50% softening, $t_{50\%}$, is presented as a function of strain for different deformation parameters. From these figures it can be seen again that the rate of post-dynamic softening is strongly dependent on the strain rate (Fig. 7(c)) and a weak function of temperature (Fig. 7(b)). Similar trends were obtained for curves simulated without static recovery (Fig. 7(a)). These results also show that beyond ε_{c} there is a strain-dependent and strain-independent range. It also reveals two kinds of transitions between these two ranges. For the first, $t_{50\%}$ gradually decreases with applied strain until it reaches a plateau and becomes independent of strain. Here we may ask ourselves: Why is it that close to the peak strain, ε_{p}, for a single-peak flow curve, the time $t_{50\%}$ is not a minimum, since the average dislocation density is a maximum at that time? The reason for this is that at ε_{p} the grain refinement is not yet finished and the number of potential nucleation sites are not at maximum. For time $t_{50\%}$ to be a minimum, the contributions of both factors, the average dislocation density and the potential nucleation sites, must be considered. This kind of transition was experimentally observed by Uranga et al. [18], who worked with very coarse-grained material (average grain

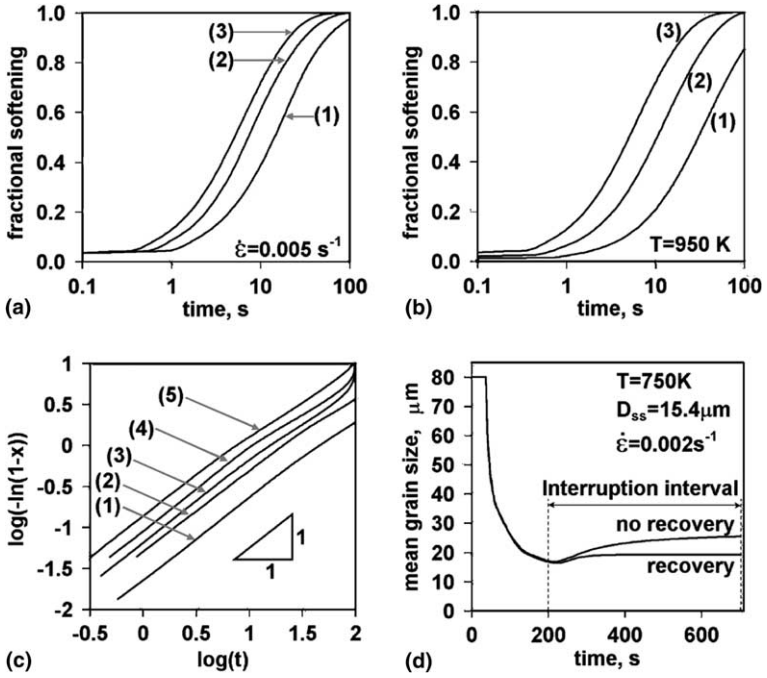

Fig. 6. Fractional softening vs. interruption time for constant strain rate and temperatures of 750 K (curve 1), 850 K (curve 2), 950 K (curve 3) (a); for constant temperature and different strain rates of 0.0005 s^{-1} (curve 1), 0.002 s^{-1} (curve 2), 0.005 s^{-1} (curve 3) (b). Avrami plots (c) for (a) and (b) with numbers from 1 to 5 representing the following pairs as a number (strain rate [s^{-1}], temperature [K]): 1 (5×10^{-3}, 950), 2 (5×10^{-3}, 850), 3 (2×10^{-3}, 950), 4 (5×10^{-3}, 750), 5 (5×10^{-4}, 950). Post-dynamic softening began at $\varepsilon = 0.8$ for Figs. (a)–(c). Comparison between the simulated evolutions of the mean grain sizes during and after deformation for simulations with and without recovery, respectively (d).

size of 806 μm). They found for their experimental data that the transition strain, ε_T, that separates both ranges is much higher than the peak strain ($\varepsilon_T/\varepsilon_p = 1.7$). Our simulations show that for very coarse-grained starting material this ratio is less sensitive to strain rate than it is in fine-grained material. The sensitivity increases when

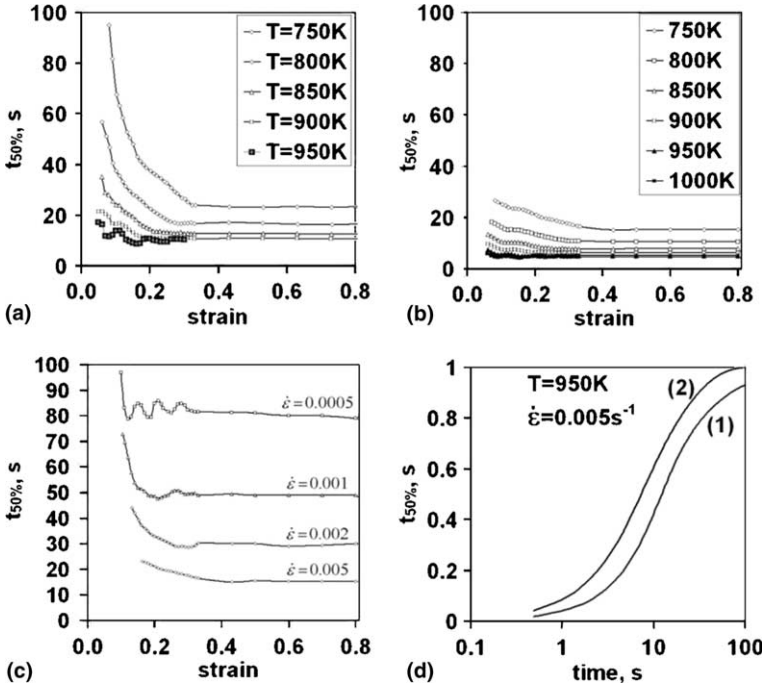

Fig. 7. Evolution of the time for 50% recrystallization with strain at different (a) temperatures without recovery ($\dot{\varepsilon} = 0.005$ s^{-1}), at different (b) temperatures with recovery ($\dot{\varepsilon} = 0.005$ s^{-1}), at constant (c) strain rates with recovery ($T = 750$ K). Comparison of softening rate (d) between simulations without static recovery (curve 1) and with static recovery (curve 2).

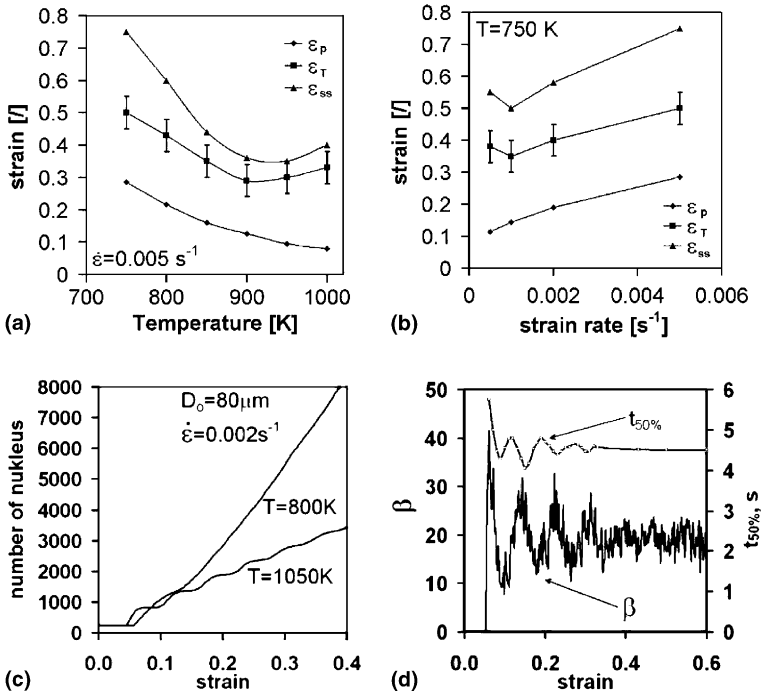

Fig. 8. Dependence of peak strain, ε_p, transition strain, ε_T and steady-state strain, ε_{ss}, on temperature (a) and strain rate (b) for $D_0 = 80$ μm. Influence of temperature on the evolution of the number of nuclei, N, with deformation at a constant strain rate and an initial mean grain size of 80 μm (c). Relation between slope $\beta = dN/d\varepsilon$ of the curve for the number of nuclei, N, vs. strain and evolution of the time for $t_{50\%}$ recrystallization with strain for a strain rate of 0.002 s^{-1} and a temperature of 750 K (d).

approaching the transition range between the single- and multiple-peak flow curves. Examples of the dependence of peak strain, transition strain and steady-state strain on temperature and strain rate for $D_0 = 80$ μm are shown in Fig. 8(a) and (b), respectively. It can be seen that ε_T lies between ε_p and ε_{ss}, which is in qualitative agreement with Uranga et al. [18]. The error bars on those two figures correspond to maximal errors, which were estimated as follows: both, flow curves and $t_{0.5}(\varepsilon)$ obtained from five repetitions of simulations do not differ more than 1%, therefore the errors of ε_{ss} and ε_p should be within this range and so they are not visible on the scale. Transition strains, ε_T, which have been determined from Fig. 8(b)–(c) when $t_{0.5}(\varepsilon)$ become independent on strain cannot be determined so accurately, but they lie within $\Delta\varepsilon = \pm 0.05$, which is denoted in the figures.

For the second type of transition, oscillations appear before the strain-independent range is reached. These oscillations were obtained for flow curves that have multiple-peak behavior. That may be attributed to the number of nuclei or nucleation sites present in the material when deformation is interrupted. It was recognized that $t_{50\%}$ is very closely related to the slope β ($\beta = dN/d\varepsilon$) of the curves shown in Fig. 8(c), where the dependence of the number of nuclei, N, on strain for the single- and multiple-peak cases is displayed. When the slope β is a minimum (minimal nucleation rate) $t_{50\%}$ is a maximum and vice versa (see Fig. 8(d)).

4. Conclusions

A CA model was developed for the simulation of multi-stage deformation and post-dynamic recrystallization for the case when dynamic recrystallization is initiated in the material during deformation. The model allows recrystallization kinetics and microstructure evolution to be simulated. At the same time, the interplay between different physical models, which can be easily incorporated in our model, can be monitored. It was recognized that there is a transition strain that separates the strain-dependent from the strain-independent range of post-dynamic softening and is larger than the critical strain for the onset of dynamic recrystallization, and could be much larger than the peak strain, ε_p. Two kinds of transition between these two ranges were revealed. For the first, $t_{50\%}$ gradually decreases with applied strain until a plateau is reached and becomes independent of strain. For the second, an oscillation appears before the strain-independent range is reached. It was also observed that the post-dynamic recrystallized fraction follows the Avrami equation with a time exponent of unity. The strong influence of recovery on the post-dynamic kinetics of recrystallization was observed. It was found that recovery shifts the softening curves toward shorter times, on the one hand, and retards the growth of grains, on the other. As a consequence, the mean size of the MDRX grains was greater when the simulations were run without static

recovery. The results of the simulations are in agreement with experimental observations [4–6,8–10,18] that the rate of metadynamic recrystallization is a strongly dependent on strain rate and weakly dependent on temperature, and that for strains larger than the transition strain, ε_T, there is no dependence on strain at all.

References

[1] Humphreys FJ, Haterly M. Recrystallization and related annealing phenomena. Oxford: Pergamon Press; 1995.
[2] Petkovic RA, Luton MJ, Jonas JJ. Acta Metall 1979;27:1633.
[3] Luton MJ, Petkovic RA, Jonas JJ. Acta Metall 1980;28:729.
[4] Sakai T. J Mat Proc Tech 1995;53:349.
[5] Kim S-I, Lee Y, Lee D-L, Yoo Y-C. Mater Sci Eng A 2003;355:384.
[6] Kim S-I, Lee Y, Jang B-L. Mater Sci Eng A 2003;357:235.
[7] Luton MJ, Sellars CM. Acta Metall 1969;17:1033.
[8] Djaic RAP, Jonas JJ. J Iron Steel Inst 1972:256.
[9] Sakai T, Ohashi M, Chiba K, Jonas JJ. Acta Metall 1988;36:1781.
[10] Roucoules C, Hodgson PD, Yue S, Jonas JJ. Metall Mater Trans A 1994;25A:389.
[11] Zhou LX, Baker TN. Mater Sci Eng A 1999;196:89.
[12] Kim S-I, Yoo Y-C. Mater Sci Eng A 2001;311:108.
[13] Belyakov A, Sakai T, Miura H, Kaibyshev R, Tsuzaki K. Acta Mater 2002;50:1547.
[14] McQueen HJ. Metall Mater Trans A 2002;33A:345.
[15] Roucoules C, Pietrzyk M, Hodgson PD. Mater Sci Eng A 2003;339:1.
[16] Sandström R, Lagneborg R. Acta Metall 1975;23:387.
[17] Sandström R, Lagneborg R. Acta Metall 1975;23:481.
[18] Uranga P, Fernàndez AI, López B, Rodrígez-Ibabe JM. Mater Sci Eng A 2003;345:319.
[19] Hesselbarth HW, Göbel IR. Acta Metall Mater 1991;39:2135.
[20] Goetz RL, Seetharaman V. Scripta Mater 1998;38:405.
[21] Wolfram S. Theory and applications of cellular automata. Singapore: World Scientific; 1986.
[22] Toffoli T, Margolus N. Cellular automata machines. Cambridge: MIT Press; 1987.
[23] Weimar JR. Simulation with cellular automata. Berlin: Logos-Verlag; 1997.
[24] Ding R, Guo ZX. Acta Mater 2001;49:3163.
[25] Kroc J. Lecture Note Comp Sci 2002;2329:773.
[26] Mecking H, Kocks UF. Acta Metall 1981;29:1865.
[27] Frost HJ, Ashby MF. Deformation-mechanism maps, the plasticity and creep of metals and ceramics. Oxford: Pergamon Press; 1982.
[28] Hurley PJ, Humphreys FJ. Acta Mater 2003;51:3779.
[29] Marx V, Reher FR, Gottstein. Acta Mater 1999;47:1219.
[30] Fernandez AI, Lopez B, Rodrígez-Ibabe JM. Scripta Mater 1999;40:54.